Dalton Transactions

ROYAL SOCIETY OF CHEMISTRY

PAPER

View Article Online
View Journal | View Issue

Cite this: *Dalton Trans.*, 2025, **54**, 10566

New members of the family of highly luminescent 1,3-bis(4-phenylpyridin-2-yl)-4,6-difluorobenzene platinum(II) complexes: exploring the effect of substituents on the 4-phenylpyridine unit†

Giulia De Soricellis,[a,b] Bertrand Carboni,[c] Véronique Guerchais,[c] J. A. Gareth Williams,[d] Daniele Marinotto,[e] Alessia Colombo,[a] Claudia Dragonetti,[a] Francesco Fagnani,*[a] Simona Fantacci[f] and Dominique Roberto[a]

Received 20th March 2025,
Accepted 26th May 2025

DOI: 10.1039/d5dt00682a

rsc.li/dalton

The synthesis and characterization of Pt{1,3-bis(4-phenylpyridin-2-yl)-4,6-difluorobenzene}Cl and Pt{1,3-bis(4-(4-methoxy-2,6-dimethylphenyl)-pyridin-2-yl)-4,6-difluorobenzene}Cl are reported, along with their molecular structure optimized by Density Functional Theory. These new *NCN*-coordinated Pt(II) complexes are both very highly luminescent in deoxygenated solution in the blue region of the spectrum: λ_{max} = 471–480 nm and Φ_{lum} = 0.89–0.98 at room temperature. Compared to the Pt{1,3-bis(pyridin-2-yl)-4,6-difluorobenzene}Cl analogue, the complex with a simple, unsubstituted phenyl ring at position 4 of the pyridinyl rings shows an improved luminescence quantum yield. However, a further enhancement is achieved with the 2,6-dimethyl-4-methoxyphenyl substituent, the steric hindrance of which inhibits the formation of bimolecular species, allowing high quantum yields to be maintained even in concentrated solutions (2×10^{-4} M).

Introduction

Luminescent platinum(II) complexes are extensively researched owing to their potential for application in nonlinear optics,[1–8] bioimaging,[9–25] sensing,[26–28] photocatalysis,[29–31] and electroluminescent devices.[32–46] The strong spin–orbit coupling (SOC) associated with the platinum atom promotes intersystem crossing to triplet excited states and their subsequent radiative decay by relaxing the spin selection rule. The phosphorescence is typically favoured by the introduction of platinum–carbon bonds within cyclometallated units, as the resulting strong ligand fields ensure that otherwise deactivating d–d excited states are destabilised, and non-radiative decay through them is suppressed.[47,48] Unlike complexes of d^6 metal ions such as Ir(III), the square planar geometry favours the formation of bimolecular states – either in the ground state (dimers or higher aggregates) or in the excited state (excimers) – thanks to Pt···Pt or ligand···ligand intermolecular interactions. These species may emit at lower energies than the isolated molecules, offering an intriguing route to deep-red/NIR-emitting materials, colour modulation according to the local concentration, and even white light emission.[42,43,49–51]

Pt(II) complexes of the *NCN*-coordinating ligand 1,3-bis(pyridin-2-yl)benzene (dpyb) are among the brightest and most efficient Pt-based emitters, apparently owing to the combination of a particularly short Pt–C bond and high rigidity, minimising non-radiative decay.[52–55] Recently, some of us studied the effect of the introduction of a polarizable π-delocalized bulky substituent on the phosphorescence properties of Pt(F_2dpyb)Cl {F_2dpybH = 1,3-bis(pyridin-2-yl)-4,6-difluorobenzene},[56] demonstrating particularly high quantum yields for **PtL^1Cl** and **PtL^2Cl** {Scheme 1; HL^1 = 1,3-bis(4-triphenylamine-pyridin-2-yl)-4,6-difluoro-benzene and HL^2 = 1,3-bis(4-mesityl-pyridin-2-yl)-4,6-difluoro-benzene}.[57,58] In this

[a]*Dipartimento di Chimica, Università degli Studi di Milano and UdR-INSTM di Milano, Via C. Golgi 19, I-20133 Milan, Italy. E-mail: francesco.fagnani@unimi.it*
[b]*Dipartimento di Chimica, Università di Pavia, Via Taramelli 12, I-27100 Pavia, Italy*
[c]*Université de Rennes 1, CNRS, ISCR (Institut des Sciences Chimiques de Rennes) - UMR 6226, F-35000 Rennes, France*
[d]*Department of Chemistry, University of Durham, South Road, Durham, DH1 3LE, UK*
[e]*Istituto di Scienze e Tecnologie Chimiche (SCITEC) "Giulio Natta", Consiglio Nazionale delle Ricerche (CNR), via C. Golgi 19, I-20133 Milan, Italy*
[f]*Istituto di Scienze e Tecnologie Chimiche "Giulio Natta" SCITEC, Consiglio Nazionale delle Ricerche (CNR), Computational Laboratory for Hybrid/Organic Photovoltaics (CLHYO), via Elce di Sotto 8, 06213 Perugia, Italy*
† Electronic supplementary information (ESI) available. See DOI: https://doi.org/10.1039/d5dt00682a

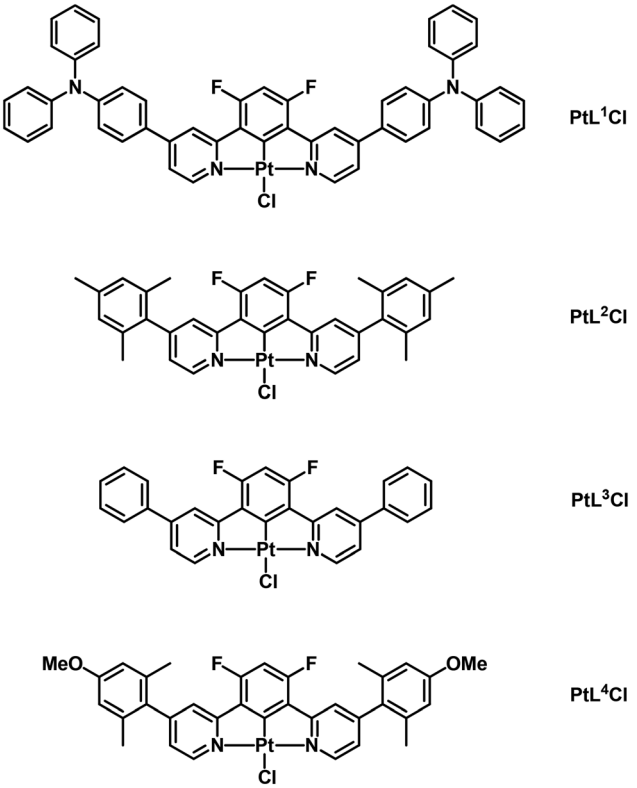

Scheme 1 Chemical structures of the investigated complexes.

context, we were curious to see the effect of the introduction of other π-delocalized groups on the 4-position of the pyridine rings. Here we describe the synthesis and properties of the complex with a simple unsubstituted phenyl group on each pyridine ring (**PtL^{3}Cl**, Scheme 1) and the related complex with a 2,6-dimethyl-4-methoxyphenyl group (**PtL^{4}Cl**). Both are highly emissive, enlarging this fascinating, brightly luminescent family of complexes based on *NCN* ligands that feature 4-phenylpyridin-2-yl units.

Results and discussion

Preparation of the new pro-ligands HL^n and of the related Pt(II) complexes

The new proligand 1,3-bis(4-phenylpyridin-2-yl)-4,6-difluorobenzene (**HL^3**) was prepared by Pd-catalysed cross-coupling of the pinacol ester of 1,3-difluoro-4,6-diboronic acid[58] with 2-chloro-4-phenylpyridine. 1,3-Bis(4-(4-methoxy-2,6-dimethylphenyl)-pyridin-2-yl)-4,6-difluorobenzene (**HL^4**) was prepared similarly using 2-chloro-4-(2,6-dimethyl-4-methoxyphenyl)-pyridine (Scheme 2). The two chlorinated reagents were likewise prepared by cross-couplings, as shown in Scheme 2. Reaction of the proligands with K_2PtCl_4 led to **PtL^{3}Cl** and **PtL^{4}Cl** in 93% and 81% yield, respectively. Full details of synthesis and characterisation are provided in the Experimental Section and in the ESI.†

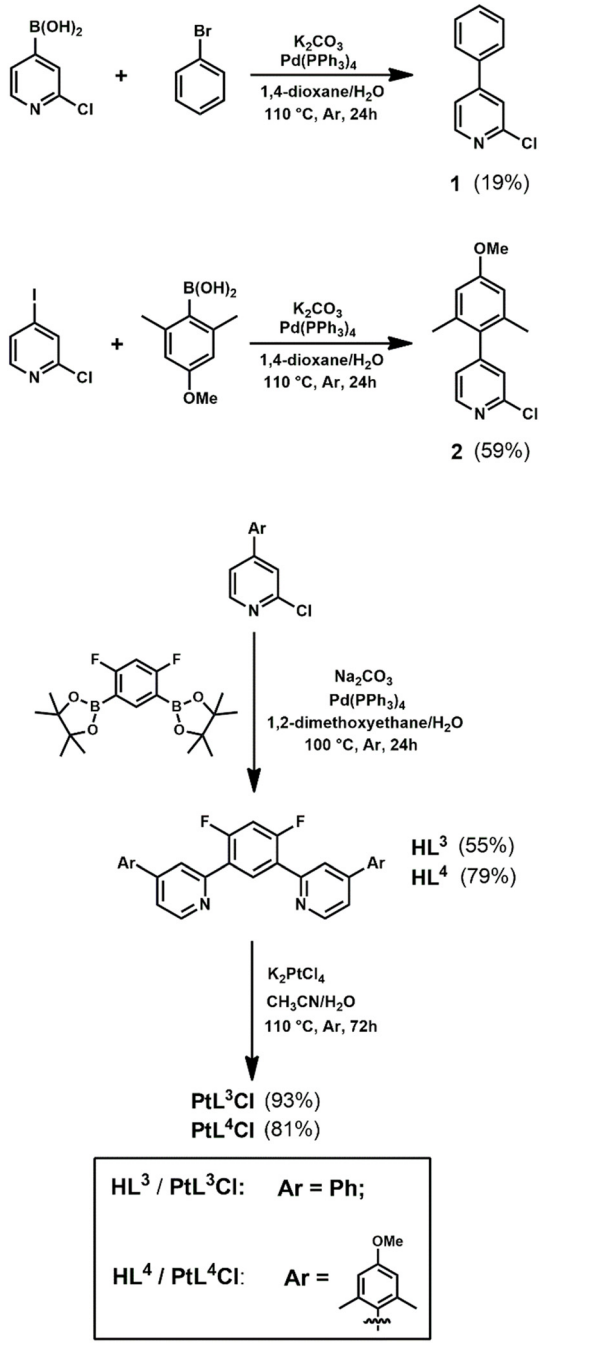

Scheme 2 Synthesis of PtL^{3}Cl and PtL^{4}Cl.

Photophysical properties

The absorption spectra of **PtL^{3}Cl** and **PtL^{4}Cl** in dichloromethane at selected concentrations between 1×10^{-6} and 1×10^{-4} M are shown in Fig. 1. There are intense bands in the range 260–320 nm, due to intraligand $^1\pi$–π^* transitions of the *NCN* ligand, and less intense bands at 340–420 nm, due to charge-transfer transitions involving the cyclometalated ligand and the metal, as for related *NCN*-coordinated platinum(II) complexes.[55–59] A weaker band at 471 and 467 nm (ε = 262 and

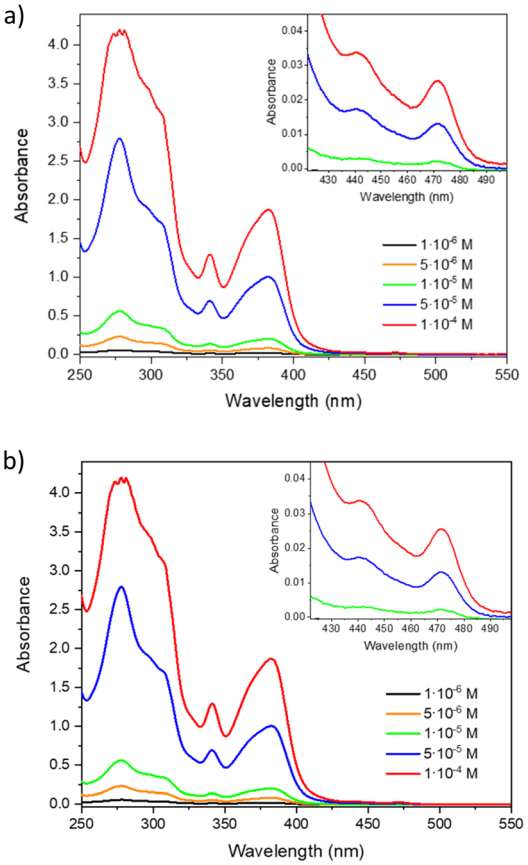

Fig. 1 Absorption spectra of **PtL^{3}Cl** (a) and **PtL^{4}Cl** (b) at the concentrations indicated, in CH_2Cl_2 at 298 K. The weak bands at longer wavelengths are shown on an expanded scale in the insets, for clarity.

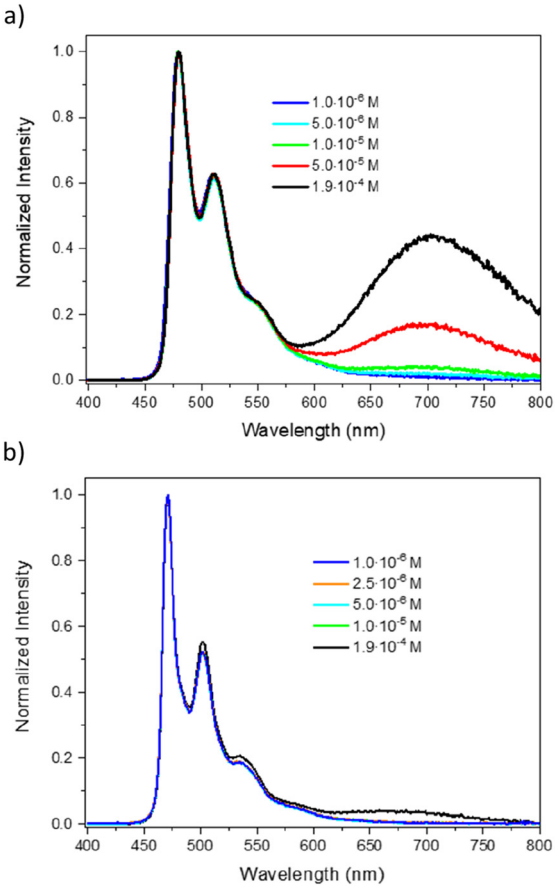

Fig. 2 Normalized emission spectra of **PtL^{3}Cl** (a; λ_{ex} = 380 nm) and **PtL^{4}Cl** (b; λ_{ex} = 377 nm) in degassed dichloromethane solution at the concentrations indicated, at 298 K.

214 M^{-1} cm^{-1}) for **PtL^{3}Cl** and **PtL^{4}Cl**, respectively (Fig. 1, insets), is attributed to the weak transition from the singlet ground state to the lowest triplet state. This formally spin forbidden $S_0 \rightarrow T_1$ transition, facilitated by the high SOC associated with the Pt centre, is close to that of the parent Pt(F_2dpyb)Cl (467 nm, 140 M^{-1} cm^{-1}). The higher extinction coefficient for this transition in **PtL^{3}Cl** and **PtL^{4}Cl** may be an indication of more efficient SOC pathways.

The normalized emission spectra of **PtL^{3}Cl** and **PtL^{4}Cl** at various concentrations in degassed CH_2Cl_2 solution at room temperature are shown in Fig. 2 (see also Fig. S4–S8 and S18–S22 in the ESI†). Upon excitation at 380 nm in dilute solution (1×10^{-6} M), **PtL^{3}Cl** displays a structured spectrum, $\lambda^{0,0}$ = 480 nm, with a vibrational progression of around 1400 cm^{-1}, attributed to emission from the T_1 state.[56] The corresponding band of **PtL^{4}Cl** is a little blue-shifted to 471 nm, very similar to that reported for the mesityl analogue **PtL^{2}Cl**[58] and for Pt(F_2dpyb)Cl.[56] In contrast, the previously investigated triphenylamine-substituted complex **PtL^{1}Cl** displayed much lower-energy emission, with λ_{max} = 562 nm.[57]

For **PtL^{3}Cl**, as the concentration is increased, a broad, structureless band progressively grows in, with λ_{max} around 704 nm (Fig. 2a), attributed to the formation of emissive, bimolecular excited states (excimers and/or aggregates).[59] For **PtL^{4}Cl**, the corresponding band – centered at 680 nm in this case – is much less intense at a given concentration (compare Fig. 2a and b), probably due to the steric hindrance of the 4-methoxy-2,6-dimethyl phenyl substituent on the pyridyl rings. The presence of the two methyl groups *ortho* to the interannular C–C bond will inhibit the attainment of the planar conformation that favours face-to-face intermolecular interactions. The corresponding band was similarly weak in the mesityl-substituted **PtL^{2}Cl**.[58]

Under the same conditions, **PtL^{1}Cl**, **PtL^{2}Cl**, and **Pt(F_2dpyb)Cl** are bright Pt(II) emitters with reported luminescence quantum yields (Φ_{lum}) of 0.90,[57] 0.97,[58] and 0.80,[56] respectively. **PtL^{3}Cl** and **PtL^{4}Cl** are similarly here to be characterized by excellent quantum yields of 0.89 and 0.98, respectively, as determined with an integrating sphere (Table 1). Under air-equilibrated conditions, the Φ_{lum} values decrease to 0.28 and 0.16, respectively, due to oxygen quenching; given the efficacy of this quenching, efficient production of singlet oxygen can be anticipated, an interesting aspect for photodynamic therapy.[19]

The formation of excimers and aggregates of Pt(*NCN*)Cl complexes typically comes at the expense of the quantum

Table 1 Photophysical parameters of **PtL^{3}Cl** and **PtL^{4}Cl**, with those of **PtL^{1}Cl**[57] and **PtL^{2}Cl**[58] also reported for comparison

Parameter[a]	**PtL^{1}Cl**	**PtL^{2}Cl**	**PtL^{3}Cl**	**PtL^{4}Cl**
$\lambda_{max,abs}$ $S_0 \rightarrow T_1$/nm [ε/M^{-1} cm^{-1}]	Not detected	467 [120]	471 [277]	467 [214]
$\lambda_{max,em}$/nm[b] monomer [excimer][c]	562 [696]	471 [680]	480 [704]	471 [680]
Φ_{lum}[d] [aerated]	0.90 [0.059]	0.97 [0.18]	0.89 [0.28]	0.98 [0.16]
Φ_{lum} (1.9×10^{-4} M)[d] [aerated]	0.66 [0.026]	0.62 [0.12]	0.53 [0.22]	0.85 [0.13]
τ/μs	104	4.8	3.5	4.5
τ/μs (1.9×10^{-4} M)	4.3	2.4	0.93	4.0
k_r[e]/s^{-1}	8.7×10^3	2.0×10^5	2.5×10^5	2.2×10^5
k_r[e]/s^{-1} (1.9×10^{-4} M)	1.5×10^5	2.6×10^5	5.7×10^5	2.1×10^5
k_{nr}[e]/s^{-1}	96×10^2	6.3×10^3	3.1×10^4	4.4×10^3
k_{nr}[e]/ s^{-1} (1.9×10^{-4} M)	7.7×10^4	1.6×10^5	5.1×10^5	3.7×10^4

[a] At a concentration of 5×10^{-6} M at 298 K in degassed CH_2Cl_2, unless otherwise indicated. [b] λ_{ex} = 422, 334, 380, and 377 nm for **PtL^{1}Cl**, **PtL^{2}Cl**, **PtL^{3}Cl**, and **PtL^{4}Cl**, respectively. [c] λ_{max} of the excimer at 1.9×10^{-4} M. [d] φ_{lum} measured with an integrating sphere. [e] Radiative and non-radiative rate constants are calculated from the quantum yields and emission decay times according to $k_r = \Phi_{lum}/\tau$ and $k_{nr} = (1 - \Phi_{lum})/\tau$.

yields.[55] For **PtL^{3}Cl** and **PtL^{4}Cl**, increasing the concentration does compromise the quantum yield, but only to a very modest extent: for instance, the values at 1.9×10^{-4} M remain remarkably high (0.53 and 0.85, respectively). Inspection of the values in Table 1, in the context also of **PtL^{1,2}Cl**, indicates that Φ_{lum} for **PtL^{4}Cl** is substantially less affected by concentration than the other three complexes. Apparently, the steric hindrance of the 4-methoxy-2,6-dimethyl phenyl substituents to the formation of bi-molecular emissive species – as noted above based on the low intensity of the low-energy excimer band – also ensures that excellent quantum yields are maintained, even at elevated concentrations.

In the literature, methods to determine the luminescence quantum yields can be divided into two main approaches: the use of an integrating sphere, or the use of standards relative to which the intensity of emission is compared.[60] We were curious to compare the Φ_{lum} values measured by means of an integrating sphere (Table 1) with those obtained relative to different standards. By using Pt(dpyb)Cl as the standard (Φ_{lum} = 0.60 in degassed CH_2Cl_2, λ_{max}^{em} = 491 nm),[52] we determined Φ_{lum} values of 0.83 and 0.93 for **PtL^{3}Cl** and **PtL^{4}Cl**, respectively, in good agreement with the values measured with the integrating sphere. By using $[Ru(bpy)_3]Cl_2$ as standard (Φ_{lum} = 0.04 in aerated H_2O; λ_{max}^{em} = 628 nm),[60] values of 0.84 and 0.71, respectively, were determined. We consider Pt(dpyb)Cl to be the more reliable standard, owing to the better match of the emissive regions and to a more comparable quantum yield.

Excited state decay measurements of **PtL^{3}Cl** in degassed CH_2Cl_2 solutions at different concentrations were performed, exciting at 374 nm and monitoring the emission at 480 nm (ESI, Table S2 and Fig. S9–S13†). The longest lifetime, 3.8 μs, is observed at the lowest concentration (1×10^{-6} M). An increase of the concentration leads to a decrease of the lifetime (3.5 and 3.3 μs at 5×10^{-6} and 1×10^{-5} M, respectively), a much lower value (0.93 μs) being obtained at 1.9×10^{-4} M. A linear Stern–Volmer relationship is observed, with a self-quenching constant k_Q of 4.3×10^9 M^{-1} s^{-1} determined from the gradient, consistent with excimer formation (*i.e.*, diffusion-controlled excited-state quenching as opposed to ground-state aggregation). Moreover, the temporal evolution of the emission intensity of the most concentrated solution at 704 nm clearly shows an initial rise at short time intervals, associated with the formation of excimers, with a τ of 0.7 μs (Fig. S14 in the ESI†). Corresponding measurements were made for **PtL^{4}Cl**, monitoring the emission intensity at 471 nm (ESI, Table S4 and Fig. S23–S27†). Again, the longest lifetime, 4.6 μs, is observed at the lowest concentration (1×10^{-6} M). In this case, the lifetime is only marginally reduced over the entire concentration range investigated (τ = 4.6, 4.5, 4.2 and 4.0 μs at 2.5×10^{-6}, 5×10^{-6}, 1×10^{-5}, and 1.9×10^{-4} M, respectively), consistent with high quantum yields being maintained at high concentrations, and with the excimer band having almost negligible intensity. In this instance, the change in lifetime is simply too small to determine the self-quenching constant reliably. However, for the most concentrated solution, the emission intensity again shows an initial rise at short time intervals after excitation (Fig. S28†), from which a time constant for excimer formation of 1.5 μs was estimated. The process is thus evidently slower than for **PtL^{3}Cl**. The effect of the 4-methoxy-2,6-dimethyl groups in hindering self-quenching and excimer formation is apparently rather larger than that associated with the mesityl groups in **PtL^{2}Cl**, wherein the lifetime declined to a greater extent with concentration (Table 1).[58] As expected, the presence of substituents on the phenyl rings of the pyridine rings reduces the propensity to form bimolecular species (see Fig. S29 in the ESI† for the plot of intensity of the lowest energy band *vs.* concentration).

The very long lifetime observed in the case of **PtL^{1}Cl**, with a triphenylamine group on the pyridines, remains unique amongst the four complexes.[57]

Radiative k_r and non-radiative k_{nr} decay constants can be estimated from the Φ_{lum} and τ values, assuming that the emitting state is formed with unit efficiency. It is clear from the values so calculated (Table 1) that the superior quantum yield of **PtL^{4}Cl** compared to **PtL^{3}Cl** originates from suppressed non-radiative processes in the former, both in dilute and concentrated solution. Meanwhile, the k_r values of **PtL$^{2-4}$Cl** are $\geq 2 \times 10^5$ s^{-1}, around 3× that of the parent unsubstituted complex Pt(dpyb)Cl, and approaching that of the "gold standard" *fac*-Ir(ppy)$_3$, for which k_r is around 4×10^5 s^{-1}.[38] It is likely that the

higher energy of the emissive triplet state in **PtL$^{2-4}$Cl** leads to a smaller S_1–T_1 energy gap ΔE_{S-T}, and hence to more efficient promotion of the formally forbidden $T_1 \rightarrow S_0$ transition (the efficiency of which is inversely related to ΔE_{S-T}[47]). The ΔE_{S-T} values estimated from the maxima of the lowest-energy absorption bands and the 0,0 component of the emission are approximately 5900 cm^{-1} for PtL^{1}Cl, compared to lower values of 5100 for PtL^{2}Cl, and 5300 cm^{-1} for PtL^{3}Cl and PtL^{4}Cl. Of course, relaxation of the spin selection rule also requires efficient mixing of metal orbitals into the excited state, to benefit from the high spin–orbit coupling associated with the metal. TD-DFT calculations on related complexes reveal heavily-mixed $d_{Pt}|\pi_L \rightarrow \pi_L^*$ states.[61,62] On the other hand, the electron-rich anilino pendants in **PtL^{1}Cl** likely render the lowest-energy excited states of intraligand character (*i.e.*, $\pi_{Ar} \rightarrow \pi_{py}^*$, where Ar = Ph_2N–C_6H_4–), suppressing the degree of metal character and leading to an abnormally low k_r and long observed lifetime τ.[61]

Computational modelling

To model the molecular structure of **PtL^{3}Cl** and **PtL^{4}Cl**, we turned to geometry optimization by Density Functional Theory (DFT). DFT calculations were performed both on the isolated complexes and on the related dimers. The dimers can be considered the simplest representative species of the aggregation phenomenon that may provide information on the packing of **PtL^{3}Cl** and **PtL^{4}Cl** in the crystal and the aggregation in solution. The monomer and the dimer geometry optimizations were performed with the Gaussian09 program package (G09)[63] by using the B3LYP exchange–correlation functional[64] integrated with the D3-BJ model[65] to include the dispersion effects in the geometry optimizations. The dichloromethane solvation effects were included through the conductor-like polarizable continuum model as implemented in G09.[66–69] All the atoms, except Pt, were described by 6-31G** basis set,[70–72] while Pt was described with the LANL2DZ basis set along with the corresponding pseudopotentials.[73] Such computational methodology has been demonstrated to be accurate for reproducing the geometry of the **PtL^{2}Cl** complex and its aggregation phenomena in solution; moreover the optimized dimer structure calculated in solution mimics the main orientation of the **PtL^{2}Cl** molecules in the crystal.[58] In Fig. 3 and 4 the optimized molecular geometries of both **PtL^{3}Cl** and **PtL^{4}Cl** monomer and dimer, respectively, are reported, showing both the front and side views for the dimers. As already observed for **(PtL^{2}Cl)$_2$**,[58] in **(PtL^{3}Cl)$_2$** and **(PtL^{4}Cl)$_2$** the two monomers are arranged in a head-to-tail configuration with respect to the Pt centers being staggered one from the other. In **(PtL^{3}Cl)$_2$** and **(PtL^{4}Cl)$_2$** the Pt···Pt distance is computed to be 4.88 Å and 6.54 Å, respectively, compared to a value of 6.31 Å for **(PtL^{2}Cl)$_2$**. In **(PtL^{3}Cl)$_2$** the presence of unsubstituted phenyls allows for a closer approach of the two monomeric units; on the contrary, in **(PtL^{4}Cl)$_2$**, the methoxy substituent in place of methyl in *para* position slightly increases the Pt···Pt distance.

The dimerization energy for the formation of **(PtL^{3}Cl)$_2$** in dichloromethane is computed to be slightly smaller than for

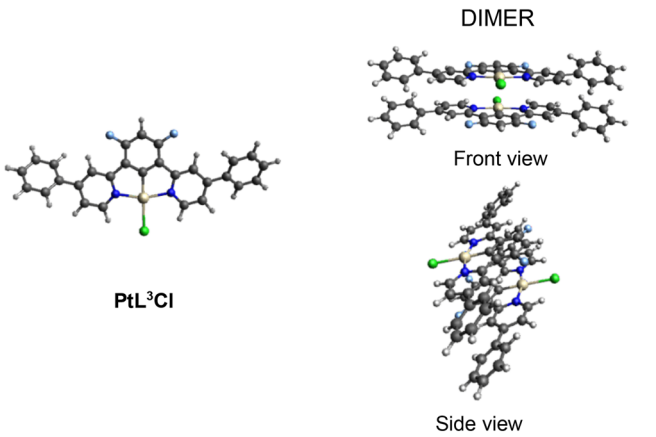

Fig. 3 Optimized molecular geometries of the monomer and dimer of **PtL^{3}Cl** in dichloromethane. Both the front and side view have been shown for the dimer.

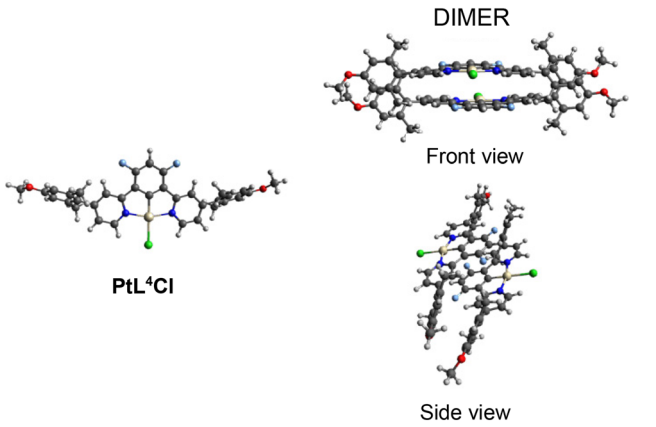

Fig. 4 Optimized molecular geometries of the monomer and dimer of **PtL^{4}Cl** in dichloromethane. Both the front and side view have been shown for the dimer.

(PtL^{2}Cl)$_2$ −43.34 kcal mol^{-1} *vs.* −47.4 kcal mol^{-1}, while that computed for **(PtL^{4}Cl)$_2$** in solution is slightly larger, at −50.5 kcal mol^{-1}. The dimerization energy provides an estimate of π···π and Pt···Pt interactions that allow the dimer to form.

Conclusion

In conclusion, two novel members of the family of 1,3-bis(4-phenylpyridin-2-yl)-4,6-difluoro-benzene Pt(II) complexes were easily prepared and well characterized. Both are highly luminescent (Φ_{lum} = 0.89–0.98) in the blue region (471–480 nm) with lifetimes of a magnitude typical for Pt(dpyb)Cl derivatives (*ca.* 4 μs). It appears that the introduction of a simple phenyl group on the position 4 of the pyridine rings is a useful way to improve the luminescence quantum yield of the parent complex Pt(F_2dpyb)Cl. A further enhancement can be achieved with a suitable functionalization of the 4-phenylpyridine

moiety. Thus, this work shows that the steric hindrance of the 4-methoxy-2,6-dimethyl phenyl moiety on the pyridinyl rings is particularly appropriate, and even better than that of a triphenylamine or mesityl group in hampering the formation of bimolecular species. It allows excellent quantum yields to be maintained even in concentrated solutions, an aspect of particular interest in future applications.

Experimental section

General comments

All reagents and solvents were used as received from the supplier. The purifications were performed through column chromatography on silica gel (Merck Geduran 60, 0.063–0.200 mm).

NMR characterizations were obtained recording on a Bruker AV III 300 MHz or AV III 400 MHz spectrometers. Chemical shifts of ^{1}H, ^{19}F and ^{13}C NMR spectra are reported in parts per million (ppm) and the coupling constants are measured in Hertz (Hz). The multiplicities of signals are listed as singlet (s), d (doublet), t (triplet), quartet (q), multiplet (m).

UV-Visible spectra were collected by a Shimadzu UV3600 spectrophotometer. Luminescence measurements were carried out in CH_2Cl_2 solution after the Freeze–Pump–Thaw (FPT) procedure necessary to remove dissolved oxygen. Photoluminescence quantum yields, Φ_{lum}, were measured using a C11347 Quantaurus Hamamatsu Photonics K.K spectrometer (see ESI† for details) or relative to the standards indicated earlier.

Steady state and time-resolved fluorescence data were obtained using a FLS980 spectrofluorimeter (Edinburg Instrument Ltd). Emission spectra were corrected for background intensity and quantum efficiency of the photomultiplier tube. Excitation spectra were corrected for the intensity fluctuation of a 450 W Xenon arc lamp. Time-resolved fluorescence measurements were performed through the time-correlated single photon counting technique with an Edinburgh Picosecond Pulsed Diode Laser (emitted wavelength 374 nm).

Synthesis of PtL^{3}Cl

HL^3 (0.10 g, 0.24 mmol) was dissolved in acetonitrile (9 mL) and a solution of K_2PtCl_4 (0.16 g, 0.38 mmol) in water (1 mL) was added. Before sealing the flask, the reaction mixture was degassed by bubbling argon through the solution for 30 minutes. The mixture was heated at 110 °C for 72 h. The obtained suspension was allowed to cool to room temperature and was filtered through a 0.45 μm Nylon membrane. The collected solid was then washed with water, MeOH and diethyl ether, and dried under vacuum to obtain the desired Pt complex as a yellow powder (121 mg, 93% yield). ^{1}H-NMR (300 MHz, $CDCl_3$, δ): 9.32 (d, J = 6.1 Hz, $^{3}J(^{195}Pt)$ = 41 Hz, 2H), 8.11 (s, 2H), 7.69–7.78 (m, 4H), 7.58 (dd, J = 8.9, 5.0 Hz, 6H), 7.49 (dd, J = 6.0, 1.9 Hz, 2H), 6.77 (t, J = 11.3 Hz, 1H). ^{19}F $\{^{1}H\}$ NMR (282.36 MHz, $CDCl_3$, δ): −108.30 (s, $^{3}J(^{195}Pt)$ = 43 Hz, 2F). ^{13}C $\{^{1}H\}$ NMR (75.48 MHz, $CDCl_3$, δ): 151.8, 136.7, 130.3, 129.4, 127.2, 120.7, 120.4. Elemental anal. calcd for $C_{28}H_{17}F_2N_2{}^{195}Pt^{35}Cl$: C, 51.74; H, 2.64; N, 4.31; Cl, 5.45; F, 5.85, Pt, 30.01; found: C, 51.83; H, 2.67; N, 4.33.

Synthesis of PtL^{4}Cl

HL^4 (0.14 g, 0.27 mmol) was dissolved in acetonitrile (11.7 mL) and a solution of K_2PtCl_4 (0.22 g, 0.53 mmol) in water (1.3 mL) was added. Argon was bubbled through the mixture for 40 minutes before sealing the reaction vessel. The reaction mixture was heated to 110 °C for 72 h. The obtained suspension was allowed to cool to room temperature and then filtered through a 0.45 μm Nylon membrane. The collected solid waswashed with water, MeOH and diethyl ether, and dried under vacuum to obtain the desired Pt complex as a yellow powder (124 mg, 81%). ^{1}H-NMR (300 MHz, $CDCl_3$, δ): 9.40 (d, J = 5.9 Hz, $^{3}J(^{195}Pt)$ = 40 Hz, 2H), 7.76 (s, 2H), 7.17 (d, J = 5.8, 2H), 6.68–6.80 (m, 5H), 3.87 (s, 6H), 2.13 (s, 12H). $^{13}C\{^{1}H\}$-NMR (75.48 MHz, $CDCl_3$, δ): 164.2, 159.4, 153.8, 151.9, 136.3, 130.7, 124.9, 124.1, 113.3, 55.2, 21.2. $^{19}F\{^{1}H\}$-NMR (282 MHz, $CDCl_3$, δ): −108.1 (s, 2F). HRMS (ESI^+): $(M + Na)^+$ calcd for $C_{34}H_{29}N_2O_2F_2{}^{35}Cl\ Na^{195}Pt$, 788.1426; found: 788.1436. Elemental anal. calcd for $C_{34}H_{29}ClF_2N_2O_2Pt$: C, 53.30; H, 3.82; N, 3.66; found: C, 53.55; H, 3.83; N, 3.64.

Author contributions

Conceptualization, D.R. and V.G.; methodology, B.C., D.M., A. C., C.D., F.F., S.F.; investigation, G.D., D.M., F.F., J.A.G.W., S.F.; resources, A.C. and C.D.; data curation, G.D., D.M., F.F., J.A.G. W., S.F.; supervision, D.R. and V.G.; writing—original draft, F. F.; writing—review and editing, G.D., B.C., V.G., J.A.G.W., D. M., A.C., C.D., F.F., S.F., D.R. All authors have read and agreed to the published version of the manuscript.

Data availability

The data supporting this article, including details on the synthesis and full characterization of the two complexes (^{1}H, ^{13}C, and ^{19}F NMR spectra, HRMS, elemental analysis, photophysical characterization), computational modelling have been included as part of the ESI.†

Conflicts of interest

There are no conflicts to declare.

Acknowledgements

Fondazione Cariplo and Regione Lombardia are acknowledged for the instrumentation bought during the SmartMatLab Centre project (2014). The work was supported by the National Interuniversity Consortium of Materials Science and Technology (Project TRI_25_073 Dragonetti and TRI_25_173

Colombo) and Università di Milano (Project PSR2023_DIP_005_PI_FTESS).

References

1 A. Colombo, C. Dragonetti, D. Marinotto, S. Righetto, D. Roberto, S. Tavazzi, M. Escadeillas, V. Guerchais, H. Le Bozec, A. Boucekkine and C. Latouche, *Organometallics*, 2013, **32**, 3890–3894.
2 D. Espa, L. Pilia, C. Makedonas, L. Marchiò, M. L. Mercuri, A. Serpe, A. Barsella, A. Fort, C. A. Mitsopoulou and P. Deplano, *Inorg. Chem.*, 2014, **53**, 1170–1183.
3 D. Espa, L. Pilia, S. Attar, A. Serpe and P. Deplano, *Inorg. Chim. Acta*, 2018, **470**, 295–302.
4 H. Zhao, E. Garoni, T. Roisnel, A. Colombo, C. Dragonetti, D. Marinotto, S. Righetto, D. Roberto, D. Jacquemin, J. Boixel and V. Guerchais, *Inorg. Chem.*, 2018, **57**, 7051–7063.
5 S. Attar, F. Artizzu, L. Marchik, D. Espa, L. Pilia, M. F. Casula, A. Serpe, M. Pizzotti, A. Orbelli-Biroli and P. Deplano, *Chem. – Eur. J.*, 2018, **24**, 10503–10512.
6 A. Colombo, C. Dragonetti, V. Guerchais and D. Roberto, *Coord. Chem. Rev.*, 2021, **446**, 214113–213133.
7 J. Boixel, A. Colombo, F. Fagnani, P. Matozzo and C. Dragonetti, *Eur. J. Inorg. Chem.*, 2022, **22**, e202200034.
8 F. Fagnani, A. Colombo, C. Dragonetti, D. Roberto, V. Guerchais, T. Roisnel, D. Marinotto and S. Fantacci, *Eur. J. Inorg. Chem.*, 2024, **27**, e202400478.
9 C.-K. Koo, K.-L. Wong, C. W.-Y. Man, Y.-W. Lam, L. K.-Y. So, H.-L. Tam, S.-W. Tsao, K.-W. Cheah, K.-C. Lau, Y.-Y. Yang, J.-C. Chen and M. H.-W. Lam, *Inorg. Chem.*, 2009, **48**, 872–878.
10 P. Wu, E. L. Wong, D. Ma, G. S. Tong, K. Ng and C. Che, *Chem. – Eur. J.*, 2009, **15**, 3652–3656.
11 V. Fernandez-Moreira, F. L. Thorp-Greenwood and M. P. Coogan, *Chem. Commun.*, 2010, **46**, 186–202.
12 Q. Zhao, C. Huang and F. Li, *Chem. Soc. Rev.*, 2011, **40**, 2508–2524.
13 E. Baggaley, J. A. Weinstein and J. A. G. Williams, *Coord. Chem. Rev.*, 2012, **256**, 1762–1785.
14 E. Baggaley, S. W. Botchway, J. W. Haycock, H. Morris, I. V. Sazanovich, J. A. G. Williams and J. A. Weinstein, *Chem. Sci.*, 2014, **5**, 879–886.
15 M. Mauro, A. Aliprandi, D. Septiadi, N. S. Kehr and L. De Cola, *Chem. Soc. Rev.*, 2014, **43**, 4144–4166.
16 K. Mitra, C. E. Lyons and M. C. T. Hartman, *Angew. Chem., Int. Ed.*, 2018, **57**, 10263–10267.
17 V. W.-W. Yam and A. S.-Y. Law, *Coord. Chem. Rev.*, 2020, **414**, 213298.
18 A. S.-Y. Law, L. C.-C. Lee, K. K.-W. Lo and V. W.-W. Yam, *J. Am. Chem. Soc.*, 2021, **143**, 5396–5405.
19 G. De Soricellis, F. Fagnani, A. Colombo, C. Dragonetti and D. Roberto, *Inorg. Chim. Acta*, 2022, **541**, 121082.
20 J. Berrones Reyes, P. S. Sherin, A. Sarkar, M. K. Kuimova and R. Vilar, *Angew. Chem., Int. Ed.*, 2023, e202310402.
21 J. Wu, B. Xu, Y. Xu, L. Yue, J. Chen, G. Xie and J. Zhao, *Inorg. Chem.*, 2023, **62**, 19142–19152.
22 E. Clancy, S. Ramadurai, S. R. Needham, K. Baker, T. A. Eastwood, J. A. Weinstein, D. P. Mulvihill and S. W. Botchway, *Sci. Rep.*, 2023, **13**, 422.
23 A. Upadhyay, A. Nepalia, A. Bera, D. K. Saini and A. R. Chakravarty, *Chem. – Asian J.*, 2023, **18**, 1–11.
24 F. Fagnani, G. De Soricellis, A. Colombo, C. Dragonetti, D. Roberto, A. di Biase, S. Fantacci and D. Marinotto, *Dyes Pigm.*, 2024, **225**, 112064.
25 R. M. Dell'Acqua, F. Fagnani, M. Wojciechowska, D. Marinotto, G. Colombo, I. Dalle-Donne, J. Trylska, S. Cauteruccio and A. Colombo, *Dalton Trans.*, 2025, **54**, 3314–3322.
26 A. Haque, H. El Moll, K. M. Alenezi, M. S. Khan and W. Y. Wong, *Materials*, 2021, **14**, 4236–4261.
27 A. S.-Y. Law, M. C.-L. Yeung and V. W.-W. Yam, *ACS Appl. Mater. Interfaces*, 2017, **9**, 41143–41150.
28 Y. Y. Ning, G. Q. Jin, M. X. Wang, S. Gao and J. L. Zhang, *Curr. Opin. Chem. Biol.*, 2022, **66**, 102097–102107.
29 M. Yoshida, K. Saito, H. Matsukawa, S. Yanagida, M. Ebina, Y. Maegawa, S. Inagaki, A. Kobayashi and M. Kato, *J. Photochem. Photobiol., A*, 2018, **358**, 334–344.
30 D. Gómez de Segura, A. Corral-Zorzano, E. Alcolea, M. T. Moreno and E. Lalinde, *Inorg. Chem.*, 2024, **63**, 1589–1606.
31 P. Domingo-Legarda, A. Casado-Sánchez, L. Marzo, J. Alemán and S. Cabrera, *Inorg. Chem.*, 2020, **59**, 13845–13857.
32 W. Sotoyama, T. Satoh, N. Sawatari and H. Inoue, *Appl. Phys. Lett.*, 2005, **86**, 153505–153507.
33 M. Cocchi, D. Virgili, V. Fattori, D. L. Rochester and J. A. G. Williams, *Adv. Funct. Mater.*, 2007, **17**, 285–289.
34 X. Yang, Z. Wang, S. Madakuni, J. Li and G. E. Jabbour, *Adv. Mater.*, 2008, **20**, 2405–2409.
35 W. Y. Wong and C. L. Ho, *Chem. Soc. Rev.*, 2009, **253**, 1709–1758.
36 C. M. Che, C. C. Kwok, S. W. Lai, A. F. Rausch, W. J. Finkenzeller, N. Y. Zhu and H. Yersin, *Chem. – Eur. J.*, 2010, **16**, 233–247.
37 J. Kalinowski, V. Fattori, M. Cocchi and J. A. G. Williams, *Coord. Chem. Rev.*, 2011, **255**, 2401–2425.
38 L. F. Gildea and J. A. G. Williams, Iridium and platinum complexes for OLEDs, in *Organic Light-Emitting Diodes: Materials, Devices and Applications*, ed. A. Buckley, Woodhead, Cambridge, 2013.
39 G. Cheng, P.-K. Chow, S. C. F. Kui, C.-C. Kwok and C.-M. Che, *Adv. Mater.*, 2013, **25**, 6765–6770.
40 C. Cebrian and M. Mauro, *Beilstein J. Org. Chem.*, 2018, **14**, 1459–1481.
41 X. Yang, H. Guo, X. Xu, Y. Sun, G. Zhou, W. Ma and Z. Wu, *Adv. Sci.*, 2019, **6**, 1801930.
42 W.-C. Chen, C. Sukpattanacharoen, W.-H. Chan, C.-C. Huang, H.-F. Hsu, D. Shen, W.-Y. Hung, N. Kungwan, D. Escudero, C.-S. Lee and Y. Chi, *Adv. Funct. Mater.*, 2020, **30**, 2002494.

43 Y.-C. Wei, S. F. Wang, Y. Hu, L.-S. Liao, D.-G. Chen, K.-H. Chang, C.-W. Wang, S.-H. Liu, W.-H. Chan, J.-L. Liao, W.-Y. Hung, T.-H. Wang, P.-T. Chen, H.-F. Hsu, Y. Chi and P.-T. Chou, *Nat. Photonics*, 2020, **14**, 570–577.
44 S.-F. Wang, B.-K. Su, X.-Q. Wang, Y.-C. Wei, K.-H. Kuo, C.-H. Wang, S.-H. Liu, L.-S. Liao, W.-Y. Hung, L.-W. Fu, W.-T. Chuang, M. Qin, X. Lu, C. You, Y. Chi and P.-T. Chou, *Nat. Photonics*, 2022, **16**, 843–850.
45 F. Fagnani, A. Colombo, C. Dragonetti, D. Roberto and D. Marinotto, *Inorg. Chim. Acta*, 2022, **532**, 120744.
46 D. Roberto, A. Colombo, C. Dragonetti, F. Fagnani, M. Cocchi and D. Marinotto, *Molecules*, 2022, **27**, 5171.
47 H. Yersin, A. F. Rausch, R. Czerwieniec, T. Hofbeck and T. Fischer, *Coord. Chem. Rev.*, 2011, **255**, 2622–2652.
48 P. T. Chou, Y. Chi, M. W. Chung and C. C. Lin, *Coord. Chem. Rev.*, 2011, **255**, 2653–2665.
49 V. Adamovich, J. Brooks, A. Tamayo, A. M. Alexander, P. I. Djurovich, B. W. D'Andrade, C. Adachi, S. R. Forrest and M. E. Thompson, *New J. Chem.*, 2002, **26**, 1171–1178.
50 M. Cocchi, J. Kalinowski, V. Fattori, J. A. G. Williams and L. Murphy, *Appl. Phys. Lett.*, 2009, **94**, 073309–073311.
51 P. Brulatti, V. Fattori, S. Muzzioli, S. Stagni, P. P. Mazzeo, D. Braga, L. Maini, S. Milita and M. Cocchi, *J. Mater. Chem. C*, 2013, **1**, 1823–1831.
52 J. A. G. Williams, A. Beeby, S. Davies, J. A. Weinstein and C. Wilson, *Inorg. Chem.*, 2003, **42**, 8609–8611.
53 S. J. Farley, D. L. Rochester, A. L. Thompson, J. A. K. Howard and J. A. G. Williams, *Inorg. Chem.*, 2005, **44**, 9690–9703.
54 J. A. G. Williams, *Chem. Soc. Rev.*, 2009, **38**, 1783–1801.
55 C. Dragonetti, F. Fagnani, D. Marinotto, A. Di Biase, D. Roberto, M. Cocchi, S. Fantacci and A. Colombo, *J. Mater. Chem. C*, 2020, **8**, 7873–7881.
56 A. F. Rausch, L. Murphy, J. A. G. Williams and H. Yersin, *Inorg. Chem.*, 2012, **51**, 312–319.
57 A. Colombo, G. De Soricellis, F. Fagnani, C. Dragonetti, M. Cocchi, B. Carboni, V. Guerchais and D. Marinotto, *Dalton Trans.*, 2022, **51**, 12161–12169.
58 A. Colombo, G. De Soricellis, C. Dragonetti, F. Fagnani, D. Roberto, B. Carboni, V. Guerchais, T. Roisnel, M. Cocchi, S. Fantacci, E. Radicchi and D. Marinotto, *J. Mater. Chem. C*, 2024, **12**, 9702–9715.
59 J. Kalinowski, M. Cocchi, L. Murphy, J. A. G. Williams and V. Fattori, *Chem. Phys.*, 2010, **378**, 47–57.
60 H. Ishida, S. Tobita, Y. Hasegawa, R. Katoh and K. Nozaki, *Coord. Chem. Rev.*, 2010, **254**, 2449–2458.
61 Aniline-based electron-rich pendants on the central aryl ring have similarly been shown to lead to enhanced intraligand charge-transfer character, at the expense of the metal, and thus to longer lifetimes: see, for example, ref. 53 and: D. L. Rochester, S. Develay, S. Zalis and J. A. G. Williams, *Dalton Trans.*, 2009, 1728–1741.
62 P. Pander, A. Sil, R. J. Salthouse, C. W. Harris, M. T. Walden, D. S. Yufit, J. A. G. Williams and F. B. Dias, *J. Mater. Chem. C*, 2022, **10**, 15084–15095.
63 M. J. Frisch, G. W. Trucks, H. B. Schlegel, G. E. Scuseria, M. A. Robb, J. R. Cheeseman, G. Scalmani, V. Barone, B. Mennucci, G. A. Petersson, H. Nakatsuji, M. Caricato, X. Li, H. P. Hratchian, A. F. Izmaylov, J. Bloino, G. Zheng, J. L. Sonnenberg, M. Hada, M. Ehara, K. Toyota, R. Fukuda, J. Hasegawa, M. Ishida, T. Nakajima, Y. Honda, O. Kitao, H. Nakai, T. Vreven, J. A. Montgomery Jr., J. E. Peralta, F. Ogliaro, M. Bearpark, J. J. Heyd, E. Brothers, K. N. Kudin, V. N. Staroverov, R. Kobayashi, J. Normand, K. Raghavachari, A. Rendell, J. C. Burant, S. S. Iyengar, J. Tomasi, M. Cossi, N. Rega, J. M. Millam, M. Klene, J. E. Knox, J. B. Cross, V. Bakken, C. Adamo, J. Jaramillo, R. Gomperts, R. E. Stratmann, O. Yazyev, A. J. Austin, R. Cammi, C. Pomelli, J. W. Ochterski, R. L. Martin, K. Morokuma, V. G. Zakrzewski, G. A. Voth, P. Salvador, J. J. Dannenberg, S. Dapprich, A. D. Daniels, O. Farkas, J. B. Foresman, J. V. Ortiz, J. Cioslowski and D. J. Fox, *Gaussian 09, Revision D.01*, Gaussian, Inc., Wallingford CT, 2009.
64 A. D. Becke, *J. Chem. Phys.*, 1993, **98**, 5648–5652.
65 S. Grimme, S. Ehrlich and L. Goerigk, *J. Comput. Chem.*, 2011, **32**, 1456–1465.
66 S. Miertus, E. Scrocco and J. Tomasi, *Chem. Phys.*, 1981, **55**, 117–129.
67 M. Cossi, V. Barone, R. Cammi and J. Tomasi, *Chem. Phys. Lett.*, 1996, **255**, 327–335.
68 V. Barone and M. Cossi, *J. Phys. Chem. A*, 1998, **102**, 1995–2001.
69 M. Cossi, N. Rega, G. Scalmani and V. Barone, *J. Comput. Chem.*, 2003, **24**, 669–681.
70 A. D. McLean and G. S. Chandler, *J. Chem. Phys.*, 1980, **72**, 5639–5648.
71 A. J. H. Wachters, *J. Chem. Phys.*, 1970, **52**, 1033.
72 A. Petersson and M. A. Al-Laham, *J. Chem. Phys.*, 1991, **94**, 6081–6090.
73 P. J. Hay and W. R. Wadt, *J. Chem. Phys.*, 1985, **82**, 299–310.